

Analytical and Numerical Buckling Analysis of Carbon Nanotube Reinforced Annular Composite Plates

E. Asadi*

Sama Technical and Vocational Training College,
Islamic Azad University, Islamshahr Branch, Iran
E-mail: esmail.asadi@gmail.com

*Corresponding author

J. E. Jam

Faculty of Materials and Manufacturing Processes,
Malek Ashtar University of Technology, Iran
E-mail: jejaam@gmail.com

Received: 25 May 2013, Revised: 14 July 2013, Accepted: 27 August 2013

Abstract: The buckling analysis of annular composite plates reinforced by carbon nanotubes (CNTs) subjected to compressive and torsional loads are studied in this paper. The Mori-Tanaka method is employed to calculate the effective elastic modulus of composites having aligned oriented straight CNTs. The effects of CNTs volume fractions, orientation angles, boundary conditions and geometric ratio of plate are discussed. The results are calculated by analytical method based on classical plate theory and finite element methods (FEMs) using ANSYS software and third order shear deformation theory for moderately thick laminated plates. It is found that the stability of plate increases as the thickness or inner to outer ratio rises and when the CNTs arranged in the circumferential direction the highest buckling load is achieved.

Keywords: Annular plates, Buckling, Carbon Nanotubes, Reinforced Composite, Third-order shear Deformation Theory

Reference: Asadi, E., Jam, J. E., "Analytical and Numerical Buckling Analysis of Carbon Nanotube Reinforced Annular Composite Plates", *Int J of Advanced Design and Manufacturing Technology*, Vol. 7/ No. 2, 2014, pp. 35-44.

Biographical notes: **E. Asadi** received his MSc in Composite engineering from Malek Ashtar University of Technology of Iran in 2013, and his BSc in Mechanical engineering from Amirkabir University of Technology, Iran. His current research focuses on buckling and vibration of nanocomposite structures. **J. E. Jam** received his PhD in Aerospace Engineering from Anna University, India in 2000. He is currently Professor at the Faculty of Materials and Manufacturing Processes, Malek Ashtar University of Technology, Tehran, Iran. His current research interest includes static and dynamic analyses of composite structures.

1 INTRODUCTION

Carbon nanotubes (CNTs) are known to possess exceptional mechanical stiffness and strength. The axial Young's modulus of both single wall carbon nanotubes (SWNTs) and multi wall carbon nanotubes (MWNTs) can be as high as 1–1.2 TPa [1], as compared to diamond at about 1.2 TPa, steel at 200 GPa, and copper at 100 GPa. Jin and Yuan [2] calculated Young's and shear modulus for SWNTs equal to 1.236 TPa and 0.492 TPa respectively, by using molecular dynamics simulations. Their tensile strength is about 100–200 GPa [3], as high as about 100 times greater as compared to annealed steel at 700 MPa and annealed copper at 200 MPa. CNTs have demonstrated the potential for order-of-magnitude increases in strength and stiffness relative to standard carbon fibres which have been used successfully in fiber reinforced polymers [4].

Composite materials reinforced by either SWNTs or MWNTs have been fabricated where significant enhancement in mechanical, electrical and thermal properties have been reported [5-7]. These mechanical properties motivate further study of possible applications for lightweight and high strength materials, especially in aerospace components. Different assumptions used for displacement fields of plates, whereupon different theories for plate analysis have been devised like, three dimensional elasticity solution, the classical laminate plate theory (CLPT), the first order and higher order shear deformation theories (FSDT and HSDT).

Considerable research has focused on the buckling analysis of composite plates under mechanical and thermal loads based on the CLPT [8-10]. Using the classical plate theory, which neglects the effects of transverse shear deformation, the calculations of the buckling loads are rather simple and generally may result in closed-form solutions. The thermal and mechanical buckling of FGM circular plates based on the first order shear deformation plate theory is studied by Najafizadeh and Hedayati [10]. Krizevsky and Stavsky [11] derived the equations of laminated annular plates by using Hamilton variational principles. Derivation of the Equilibrium and stability equations of a FGM circular plate under thermal loads, based on the third order shear deformation (TSDT) plate theory is carried out by Najafizadeh and Heydari [12]. They concluded that the critical buckling temperature for the FGM plate is generally lower than the corresponding value for the homogeneous circular plate and transverse shear deformation has considerable effect on the critical buckling temperature, especially for a thick plate.

In other article, Najafizadeh and Heydari used the higher order shear deformation plate theory (HSDT) to study the buckling of FGM circular plates under uniform radial compression [13]. Ma and Wang [14]

studied nonlinear bending and post buckling of a functionally graded circular plate under mechanical and thermal loadings based on the von Karman plate theory. Also Singhatanadgid and Ungbhakorn [15] derived the scaling laws for buckling of polar orthotropic annular plates subjected to radial compressive and torsional loads. The buckling loads obtained from the scaling laws are identical to those of the theoretical solution.

Axisymmetric bending and buckling of perfect functionally graded solid circular plates based on the unconstrained third-order shear deformation plate theory are studied by Saidi et al., [16]. Ozakca et al., obtained the buckling analysis of circular and annular plates using the finite element method (FEM) [17], [18]. The results illustrate that the FEMs can be used with confidence for the buckling analysis of circular and annular plates.

In this paper, buckling behaviour of composite circular and annular plates reinforced by carbon nanotubes, subjected to compressive and torsional loads on the inner and outer edges is presented. The material properties of composite plates reinforced by single-walled carbon nanotubes are obtained using the Mori-Tanaka method and the results are obtained with three different methods including classical laminate plate theory, third order shear deformation theory and ANSYS software. Moreover the effects of CNTs arrangement, CNTs volume fraction, boundary condition and aspect ratio of plate on critical buckling loads are discussed.

2 MATERIAL PROPERTIES

A major step in the development of CNT composites is to obtain their mechanical properties as accurately as possible. It can be seen from the literature that huge efforts have been dedicated to this specific field and investigations are still ongoing [19]-[21]. Due to its simplicity and accuracy even at high volume fractions of the inclusions, the Mori-Tanaka method [19] is employed in this study. CNTs are assumed to be aligned and straight with uniform dispersion in polymer matrix and the bonding at the nanotube-polymer interface is taken to be perfect. The elastic behaviour of an elementary cell of the composite material can be expressed as [19]:

$$\begin{bmatrix} \sigma_{11} \\ \sigma_{22} \\ \sigma_{33} \\ \tau_{23} \\ \tau_{13} \\ \tau_{12} \end{bmatrix} = \begin{bmatrix} n & l & l & 0 & 0 & 0 \\ l & k+m & k-m & 0 & 0 & 0 \\ l & k-m & k+m & 0 & 0 & 0 \\ 0 & 0 & 0 & 2m & 0 & 0 \\ 0 & 0 & 0 & 0 & 2p & 0 \\ 0 & 0 & 0 & 0 & 0 & 2p \end{bmatrix} \begin{bmatrix} \varepsilon_{11} \\ \varepsilon_{22} \\ \varepsilon_{33} \\ \varepsilon_{23} \\ \varepsilon_{13} \\ \varepsilon_{12} \end{bmatrix} \quad (1)$$

Where $k, l, m, n,$ and p are the Hill's elastic moduli, σ_{ij} and ε_{ij} are the stress and strain components, respectively. n is the uniaxial tension modulus, k is the plane-strain bulk modulus, l is the associated cross modulus, m is the transverse shear modulus, and p is the axial shear modulus, respectively, as specified in Ref. [19]. A composite with a CNTs volume fraction c_r , matrix Young's modulus E_m , and the Poisson's ratio ν_m is considered. Using the Mori-Tanaka method, the Hill's elastic moduli are found to be:

$$\begin{aligned}
 k &= \frac{E_m \{E_m c_m + 2k_r (1 + \nu_m) [1 + c_r (1 - 2\nu_m)]\}}{2(1 + \nu_m) [E_m (1 + c_r - 2\nu_m) + 2c_m k_r (1 - \nu_m - 2\nu_m^2)]} \\
 l &= \frac{E_m \{c_m \nu_m [E_m + 2k_r (1 + \nu)] + 2c_r l_r (1 - \nu_m^2)\}}{(1 + \nu_m) [2c_m k_r (1 - \nu_m - 2\nu_m^2) + E_m (1 + c_r - 2\nu_m)]} \\
 n &= \frac{E_m^2 c_m (1 + c_r - c_m \nu_m) + 2c_m c_r (k_r n_r - l_r^2) (1 + \nu_m)^2 (1 - 2\nu_m)}{(1 + \nu_m) \{2c_m k_r (1 - \nu_m - 2\nu_m^2) + E_m (1 + c_r - 2\nu_m)\}} + \\
 &\quad \frac{E_m [2c_m^2 k_r (1 - \nu_m) + c_r n_r (1 - 2\nu_m + c_r) - 4c_m l_r \nu_m]}{2c_m k_r (1 - \nu_m - 2\nu_m^2) + E_m (1 + c_r - 2\nu_m)} \\
 p &= \frac{E_m [E_m c_m + 2(1 + c_r) p_r (1 + \nu_m)]}{2(1 + \nu_m) [E_m (1 + c_r) + 2c_m p_r (1 + \nu_m)]} \\
 m &= \frac{E_m [E_m c_m + 2m_r (3 + c_r - 4\nu_m) (1 + \nu_m)]}{2(1 + \nu_m) \{E_m [c_m + 4c_r (1 - \nu_m)] + 2m_r c_m (3 + c_r - 4\nu_m^2)\}} \quad (2)
 \end{aligned}$$

Where $k_r, l_r, m_r, n_r,$ and p_r are the Hill's elastic moduli for the CNTs.

Table 1 Elastic properties of SWNTs as composite's reinforcing phase and polystyrene as a matrix [1]

Material Properties	Matrix phase	SWNTs
Isotropic Young's modulus (E_m)	1.9 GPa	-
Poisson's ratio (ν_m)	0.3	-
k_r	-	30 GPa
l_r	-	10 GPa
m_r	-	1 GPa
n_r	-	450 GPa
p_r	-	1 GPa

The composite plate is composed of polystyrene as a matrix and the CNTs are modeled as long, transversely isotropic fibres based on the analytical result of Popov et al. [1]. The elastic properties of SWNTs and polystyrene matrix are listed in Table 1. The reduced transformed stiffness coefficient for the matrix is [22]:

$$\bar{Q}_{ij} = [T] [Q_{ij}] [T]^{-1} \quad (3)$$

Where $[T]$ is the transformed matrix which is given by:

$$[T] = \begin{bmatrix} \cos^2 \theta & \sin^2 \theta & 0 & 0 & 0 & -\sin 2\theta \\ \sin^2 \theta & \cos^2 \theta & 0 & 0 & 0 & \sin 2\theta \\ 0 & 0 & 1 & 0 & 0 & 0 \\ 0 & 0 & 0 & \cos \theta & \sin \theta & 0 \\ 0 & 0 & 0 & -\sin \theta & \cos \theta & 0 \\ \sin \theta \cos \theta & -\sin \theta \cos \theta & 0 & 0 & 0 & \cos^2 \theta - \sin^2 \theta \end{bmatrix} \quad (4)$$

3 ANALYTICAL SOLUTION

The CLPT is used to work out the analytical solution as it is simply used for moderate thick cross ply laminated plates. According to the Fig. 1, 'a' and 'b' are the radii of inner and outer edges and h denotes the thickness of the plate respectively. The boundary condition on edges can be simply supported or clamped. Annular composite plate is subjected to the uniform compressive and torsional loads along inner and outer edges ($p_i, p_o,$ and Q_s respectively).

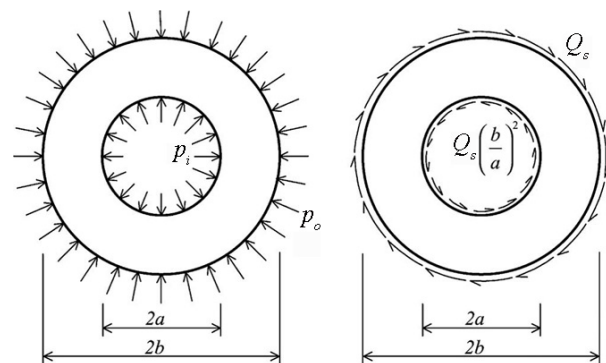


Fig. 1 Annular plate under torsional and compressive loads

The total potential energy of the plate in as much as the internal strain and the surface traction is given by [23]:

$$\Pi = \int_V \{\varepsilon\}^T \{\sigma\} dV + \int_A \{\varphi\}^T \{t\} dA \quad (5)$$

The first term in the right hand side of Eq. (5) is the strain energy which V denoting the volume of the plate. The second term produced by surface traction and A is the portion of plate surface over which tractions are prescribed. $\{\varphi\}$ is the displacement vector and $\{t\}$ is the surface traction. The constitutive relating stress and strain can be written as [22]:

$$\{\sigma\} = [C] \{\varepsilon\} \quad (6)$$

Where $[C]$ is the elastic tensor whose components are given by [22]:

$$\begin{aligned} C_{11} &= \sum_{k=1}^n [\bar{Q}_{rr}]_K, \quad C_{22} = \sum_{k=1}^n [\bar{Q}_{\theta\theta}]_K, \quad C_{12} = \sum_{k=1}^n [\bar{Q}_{r\theta}]_K \\ C_{66} &= \sum_{k=1}^n [\bar{Q}_{ss}]_K, \quad C_{16} = \sum_{k=1}^n [\bar{Q}_{rs}]_K, \quad C_{26} = \sum_{k=1}^n [\bar{Q}_{s\theta}]_K \end{aligned} \quad (7)$$

Where k denotes the number of the layer. According to Eqs. (6) and (7), the strain energy can be written as:

$$U = \frac{1}{2} \int_R [\varepsilon_r \quad \varepsilon_\theta \quad \gamma_{r\theta}] \begin{bmatrix} \bar{Q}_{rr} & \bar{Q}_{r\theta} & \bar{Q}_{rs} \\ \bar{Q}_{r\theta} & \bar{Q}_{\theta\theta} & \bar{Q}_{s\theta} \\ \bar{Q}_{rs} & \bar{Q}_{s\theta} & \bar{Q}_{ss} \end{bmatrix} \begin{bmatrix} \varepsilon_r \\ \varepsilon_\theta \\ \gamma_{r\theta} \end{bmatrix} dV \quad (8)$$

The relations between the strain and the displacement for the CLPT are given by [23]:

$$\begin{aligned} \varepsilon_r &= \frac{\partial u_r}{\partial r} = \frac{\partial u_{r0}}{\partial r} - z \frac{\partial^2 w}{\partial r^2} \\ \varepsilon_\theta &= \frac{1}{r} \frac{\partial u_\theta}{\partial \theta} + \frac{u_r}{r} = \frac{1}{r} \frac{\partial u_{\theta 0}}{\partial \theta} + \frac{u_{r0}}{r} - \frac{z}{r^2} \frac{\partial^2 w}{\partial \theta^2} - \frac{z}{r} \frac{\partial w}{\partial r} \\ \varepsilon_{r\theta} &= \frac{1}{2} \left(\frac{1}{r} \frac{\partial u_{r0}}{\partial \theta} - \frac{\partial u_{\theta 0}}{\partial r} - \frac{u_{\theta 0}}{r} \right) - \frac{2z}{r} \frac{\partial^2 w}{\partial r \partial \theta} + \frac{2z}{r^2} \frac{\partial w}{\partial \theta} \end{aligned} \quad (9)$$

Where u_{r0} and $u_{\theta 0}$ are the displacements of the mid-plane in r and θ directions respectively which are assumed to be zero because there is no coupling between the in-plane and the out-of-plane displacements. $w(r, \theta)$ indicates the displacement in z direction or the lateral deflection of the composite plate. Substituting Eq. (9) into Eq. (8) yields:

$$\begin{aligned} U &= \frac{1}{2} \int_0^{2\pi} \int_a^b \left[(D_r + D_\theta) \left(\frac{\partial^2 w}{\partial r^2} \right)^2 + 2D_1 \left(\frac{\partial^2 w}{\partial r^2} \right) \left\{ \frac{1}{r^2} \left(\frac{\partial^2 w}{\partial \theta^2} \right) + \frac{1}{r} \left(\frac{\partial w}{\partial r} \right) \right\} + \right. \\ &\left. (D_r + D_\theta) \left\{ \frac{1}{r^2} \left(\frac{\partial^2 w}{\partial \theta^2} \right) + \frac{1}{r} \left(\frac{\partial w}{\partial r} \right) \right\}^2 + (D_r + 2D_{r\theta}) \left\{ \frac{\partial}{\partial r} \left(\frac{1}{r} \frac{\partial w}{\partial r} \right) \right\}^2 \right] r dr d\theta \end{aligned} \quad (10)$$

Where D_{ij} is the bending stiffness matrix which its elements are expressed as [15]:

$$\begin{aligned} D_r &= \frac{E_r h^3}{12(1-\nu_r \nu_\theta)} & D_\theta &= \frac{E_\theta h^3}{12(1-\nu_r \nu_\theta)} \\ D_{r\theta} &= \frac{Gh^3}{6} & D_l &= \nu_\theta D_r = \nu_r D_\theta \end{aligned} \quad (11)$$

The surface traction is obtained as:

$$W = \frac{1}{2} \int_0^{2\pi} \int_a^b \left(N_r r [w_{,r}]^2 + \frac{N_\theta}{r} [w_{,\theta}]^2 + \frac{2Q_s b^2}{r^2} w_{,r} w_{,\theta} \right) dr d\theta \quad (12)$$

Where N_r and N_θ are the resultant forces in r and θ directions respectively, and comma indicates the partial derivative. According to the Levy solution [23], it is important to find suitable function for the lateral deflection. It is assumed that the lateral deflection can be written as the following separate function of r and θ variables [15]:

$$w(r, \theta) = f(r)g(\theta) \quad (13)$$

For the simply-supported boundary conditions on two edges (S-S), the lateral deflection is written as [15]:

$$w = \left(\frac{r}{a} - 1 \right)^i \left(\frac{r}{b} - 1 \right)^j \sum_{m=0}^M r^m (A_m \sin n\theta + B_m \cos n\theta) \quad (14)$$

The value of i and j depends on a kind of boundary condition. If both inner and outer radii have clamped edges, i and j are supposed to be 2 and if they have simple edges, i and j are one and for the case in which inner radius has simple edge and outer has clamped one, i is 1 and j is 2. Based on the minimum total potential energy, the plate has stable state when [23]:

$$\frac{\partial \Pi}{\partial A_m} = 0 \quad \frac{\partial \Pi}{\partial B_m} = 0 \quad (15)$$

Where A_m and B_m are the deflection amplitude, and n and m are the number of half sine waves in r and θ directions, respectively. Substituting the solution $w(r, \theta)$ from Eq. (14) into Eq. (10) and Eq. (12) leads to the set of equation which is arranged in the form of a generalized eigenvalue problem as:

$$\begin{bmatrix} f_1 & f_2 \\ f_3 & f_4 \end{bmatrix} \begin{bmatrix} A_m \\ B_m \end{bmatrix} = 0 \quad (16)$$

Where $f_1, f_2, f_3,$ and f_4 are function of material properties and plate dimensions.

4 FINITE ELEMENT METHOD

For a moderately thick plate, using a higher order shear deformation theory would lead to better results. In the

3rd order shear deformation theory developed by Reddy [24], [25] the strain equations would not need a shear correction factor which is required in the first order shear deformation theory. The theory of Reddy used in the present study is based on the following displacement field.

$$\begin{aligned}
 u(r, \theta, z) &= u_0(r, \theta) + zu_1(r, \theta) + z^2u_2(r, \theta) + z^3u_3(r, \theta) \\
 v(r, \theta, z) &= v_0(r, \theta) + zv_1(r, \theta) + z^2v_2(r, \theta) + z^3v_3(r, \theta) \\
 w(r, \theta) &= w_0(r, \theta)
 \end{aligned}
 \tag{17}$$

Here u , v , and w denote the displacement components in the r , θ , and z directions, respectively. These equations can be reduced by satisfying the stress-free conditions on the top and bottom faces of the plate, which are equivalent to $\epsilon_{rz} = \epsilon_{\theta z} = 0$ at $z = h/2$. Thus,

$$\begin{cases}
 u = u_0 + zu_1 - \frac{4z^3}{3h^2}(u_1 + w_{0,r}) \\
 v = v_0 + zv_1 - \frac{4z^3}{3h^2}(v_1 + w_{0,r}) \\
 w = w_0
 \end{cases}
 \tag{18}$$

Substituting Eq. (18) into nonlinear strain-displacement relations (Eq. (9)) gives the kinematic relations as:

$$\begin{aligned}
 \begin{bmatrix} \epsilon_r \\ \epsilon_\theta \\ \epsilon_{r\theta} \end{bmatrix} &= \begin{bmatrix} \epsilon_r^0 \\ \epsilon_\theta^0 \\ \epsilon_{r\theta}^0 \end{bmatrix} + z \begin{bmatrix} k_r \\ k_\theta \\ k_{r\theta} \end{bmatrix} + z^3 \begin{bmatrix} k_1 \\ k_2 \\ k_3 \end{bmatrix} \\
 \begin{bmatrix} \epsilon_{rz} \\ \epsilon_{\theta z} \end{bmatrix} &= \begin{bmatrix} \epsilon_{rz}^0 \\ \epsilon_{\theta z}^0 \end{bmatrix} + z^2 \begin{bmatrix} k_{rz} \\ k_{\theta z} \end{bmatrix}
 \end{aligned}
 \tag{19}$$

Where

$$\begin{aligned}
 \begin{bmatrix} \epsilon_r^0 \\ \epsilon_\theta^0 \\ \epsilon_{r\theta}^0 \end{bmatrix} &= \begin{bmatrix} u_{0,r} + \frac{1}{2}w_{0,r}^2 \\ \frac{u_0}{r} + \frac{1}{r}v_{0,\theta} + \frac{1}{2}\left(\frac{1}{r}w_{0,r}\right)^2 \\ \frac{1}{r}u_{0,\theta} + v_{0,r} - \frac{v_0}{r} + \frac{1}{r}w_{0,r}w_{0,\theta} \end{bmatrix} \\
 \begin{bmatrix} k_r \\ k_\theta \\ k_{r\theta} \end{bmatrix} &= \begin{bmatrix} u_{1,r} \\ \frac{1}{r}v_{1,\theta} + \frac{u_1}{r} \\ \frac{1}{r}u_{1,\theta} + v_{1,r} - \frac{v_1}{r} \end{bmatrix}
 \end{aligned}$$

$$\begin{aligned}
 \begin{bmatrix} k_1 \\ k_2 \\ k_3 \end{bmatrix} &= \begin{bmatrix} \frac{-4}{3h^2}(u_{1,r} + w_{0,r}) \\ \frac{-4}{h^2}\left(\frac{1}{r}v_{1,\theta} + \frac{1}{r^2}w_{0,\theta\theta} + \frac{u_1}{r} + \frac{1}{r}w_{0,r}\right) \\ \frac{-4}{3h^2}\left(\frac{1}{r}u_{1,\theta} + \frac{2}{r}w_{0,r\theta} + v_{1,r} - \frac{2}{r^2}w_{0,\theta} - \frac{v_1}{r}\right) \end{bmatrix} \\
 \begin{bmatrix} \epsilon_{rz}^0 \\ \epsilon_{\theta z}^0 \end{bmatrix} &= \begin{bmatrix} u_1 + w_{0,r} \\ v_1 + \frac{1}{r}w_{0,\theta} \end{bmatrix} \\
 \begin{bmatrix} k_{rz} \\ k_{\theta z} \end{bmatrix} &= \begin{bmatrix} \frac{-4}{h^2}(u_1 + w_{0,r}) \\ \frac{-4}{h^2}\left(v_1 + \frac{1}{r}w_{0,\theta}\right) \end{bmatrix}
 \end{aligned}
 \tag{20}$$

And it can be expressed in the following form:

$$\{\epsilon\} = ([d^0] + z[d^1] + z^2[d^2] + z^3[d^3])\{\phi\}
 \tag{21}$$

Where, $\{\phi\}^T = \langle u_0 \ v_0 \ w_0 \ \varphi_x \ \varphi_y \rangle$, and the matrix $[d^i]$ (derivation matrix) is:

$$[d^0] = \begin{bmatrix} \frac{\partial}{\partial x} & 0 & \frac{1}{2}w_{0,x} & \frac{\partial}{\partial x} & 0 & 0 \\ 0 & \frac{\partial}{\partial y} & \frac{1}{2}w_{0,y} & \frac{\partial}{\partial y} & 0 & 0 \\ 0 & 0 & \frac{\partial}{\partial y} & 0 & 1 & 0 \\ 0 & 0 & \frac{\partial}{\partial x} & 1 & 0 & 0 \\ \frac{\partial}{\partial y} & \frac{\partial}{\partial x} & w_{0,y} & \frac{\partial}{\partial x} & 0 & 0 \end{bmatrix}$$

$$[d^1] = \begin{bmatrix} 0 & 0 & 0 & \frac{\partial}{\partial x} & 0 & 0 \\ 0 & 0 & 0 & 0 & \frac{\partial}{\partial y} & 0 \\ 0 & 0 & 0 & 0 & 0 & 0 \\ 0 & 0 & 0 & 0 & 0 & 0 \\ 0 & 0 & 0 & \frac{\partial}{\partial y} & \frac{\partial}{\partial x} & 0 \end{bmatrix}$$

$$[d^2] = -\frac{4}{h^2} \begin{bmatrix} 0 & 0 & 0 & 0 & 0 \\ 0 & 0 & 0 & 0 & 0 \\ 0 & 0 & \frac{\partial}{\partial y} & 0 & 1 \\ 0 & 0 & \frac{\partial}{\partial x} & 1 & 0 \\ 0 & 0 & 0 & 0 & 0 \end{bmatrix}$$

$$[d^3] = \begin{bmatrix} 0 & 0 & w_{0,x} & \frac{\partial}{\partial x} & \frac{\partial}{\partial x} & 0 \\ 0 & 0 & w_{0,y} & \frac{\partial}{\partial y} & 0 & \frac{\partial}{\partial y} \\ 0 & 0 & 0 & 0 & 0 & 0 \\ 0 & 0 & 0 & 0 & 0 & 0 \\ 0 & 0 & 2w_{0,y} & \frac{\partial}{\partial x} & \frac{\partial}{\partial y} & \frac{\partial}{\partial x} \end{bmatrix} \quad (22)$$

After achieving the variation of the total potential energy of the plate and the surface traction from Eqs. (5) and (12) respectively, the displacement is interpolated by [26]:

$$\{\phi\} = [N] \{\Phi^{(e)}\} \quad (23)$$

Where $\{\Phi^{(e)}\}$ is the vector of unknown nodal values and the $[B^i]$ matrix is given by [26]:

$$[B^i] = [d^i] [N] \quad (24)$$

The shape function matrix $[N]$ is [26]:

$$[N] = \begin{bmatrix} N_1 & 0 & 0 & 0 & 0 & \dots & \dots & \dots & N_8 & 0 & 0 & 0 & 0 \\ 0 & N_1 & 0 & 0 & 0 & \dots & \dots & \dots & 0 & N_8 & 0 & 0 & 0 \\ 0 & 0 & N_1 & 0 & 0 & \dots & \dots & \dots & 0 & 0 & N_8 & 0 & 0 \\ 0 & 0 & 0 & N_1 & 0 & \dots & \dots & \dots & 0 & 0 & 0 & N_8 & 0 \\ 0 & 0 & 0 & 0 & N_1 & \dots & \dots & \dots & 0 & 0 & 0 & 0 & N_8 \end{bmatrix} \quad (25)$$

Where N_1 to N_8 are the Serendipity element shape functions. Also the displacement in the case of each element is given by:

$$\{\Phi^{(e)}\}^T = \langle u_0^{(1)} v_0^{(1)} w_0^{(1)} \psi_x^{(1)} \psi_y^{(1)} \dots u_0^{(8)} v_0^{(8)} w_0^{(8)} \psi_x^{(8)} \psi_y^{(8)} \rangle \quad (26)$$

Substituting Eqs. (23) and (24) into the variation of the total potential energy (Eq. (5)) yields:

$$\left(\int_V \left([B^0]^T + z [B^1]^T + z^2 [B^2]^T + z^3 [B^3]^T \right) [\bar{Q}] \times \left([B^0] + z [B^1] + z^2 [B^2] + z^3 [B^3] \right) dV \right) \{\Phi^{(e)}\} \quad (27)$$

$$- \int_A [N]^T \{t\} dA \{\Phi^{(e)}\} = 0$$

The stiffness matrix and the load vector for each element are given by:

$$[K^{(e)}] = \int_V \left([B^0]^T + z [B^1]^T + z^2 [B^2]^T + z^3 [B^3]^T \right) [\bar{Q}] \times \left([B^0] + z [B^1] + z^2 [B^2] + z^3 [B^3] \right) dV \quad (28)$$

$$\{W^{(e)}\} = \int_A [N]^T \{t\} dA \quad (29)$$

According to Bodyanski method, the stress with respect to the strain is plotted and the region where the slope of the curve increases sharply denotes the critical buckling load.

5 RESULTS AND DISCUSSIONS

The buckling of an annular composite plate reinforced by CNTs is studied. The results are obtained with three different methods including classical laminate plate theory, third order shear deformation theory and ANSYS software for three different kinds of boundary conditions, and the effects of boundary conditions are perused on the critical loads. Fig. 2 is the plot for a plate which is under torsional moment on inner and outer radius. The effect of plate's aspect ratio and CNTs volume fraction on the torsional critical load is illustrated. The buckling load declines at low volume fractions, although the critical load rises along with volume fraction.

The most stable state is achieved as a consequence of being clamped edges on both inner and outer radius. In addition simple edges on both inner and outer radius cause to lowest critical moment. Also the effect of the thickness-to-inner radius ratio on the critical buckling torsional load for different CNTs volume fraction is shown in Fig. 3. The critical buckling load goes up exponentially and the slope of the curves increases sharply at high volume fractions as the thickness of plate rises. This figure is also drawn for three boundary conditions and it follows the same pattern as the previous figure.

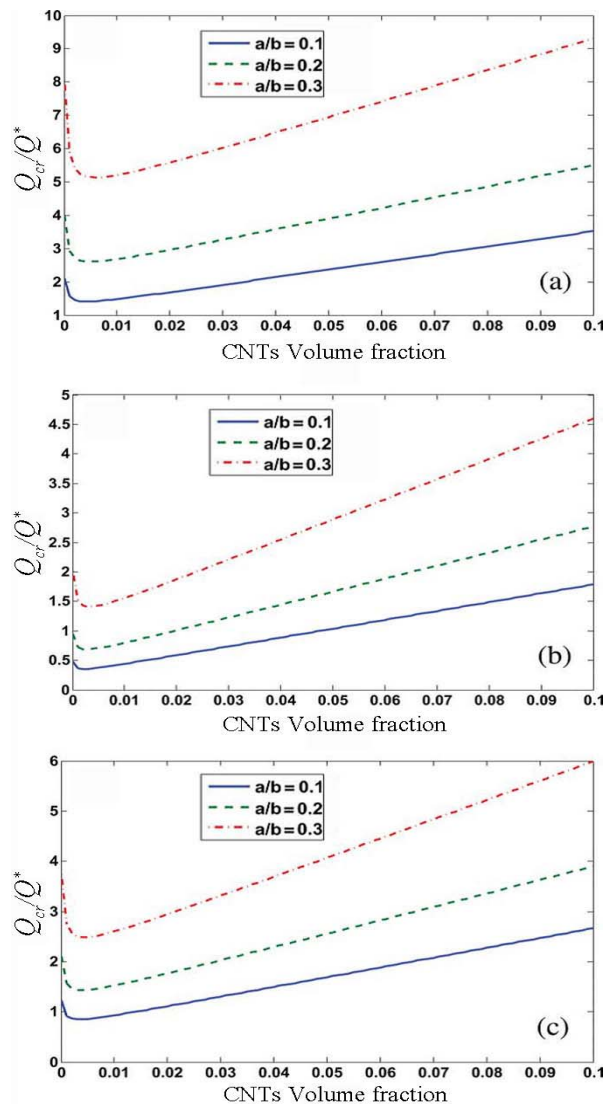


Fig. 2 The effect of CNTs volume fraction and aspect ratio on the torsional buckling loads for circular/annular composite plate for different boundary conditions (a) (C-C), (b) (S-C), (c) (S-S)

Table 2 shows a comparison between the results of the analytical solution and FEMs (TSDT and ANSYS) while the plate is subjected to compressive load. The highest critical axial buckling load occurs at $C_r=0.1$ for each aspect ratio (inner to outer radius ratio). Similar to Fig. 2 the effect of aspect ratio and CNTs volume fraction on the compressive critical load is illustrated in Fig. 4. This figure is drawn for three aspect ratios. What is more, the plate would be more stable if the ratio of inner-to-outer radius doubles. Also Fig. 5 follows the same pattern as Fig. 3 and shows the effect of the thickness-to-inner radius ratio on the critical buckling compressive load for different CNTs volume fraction.

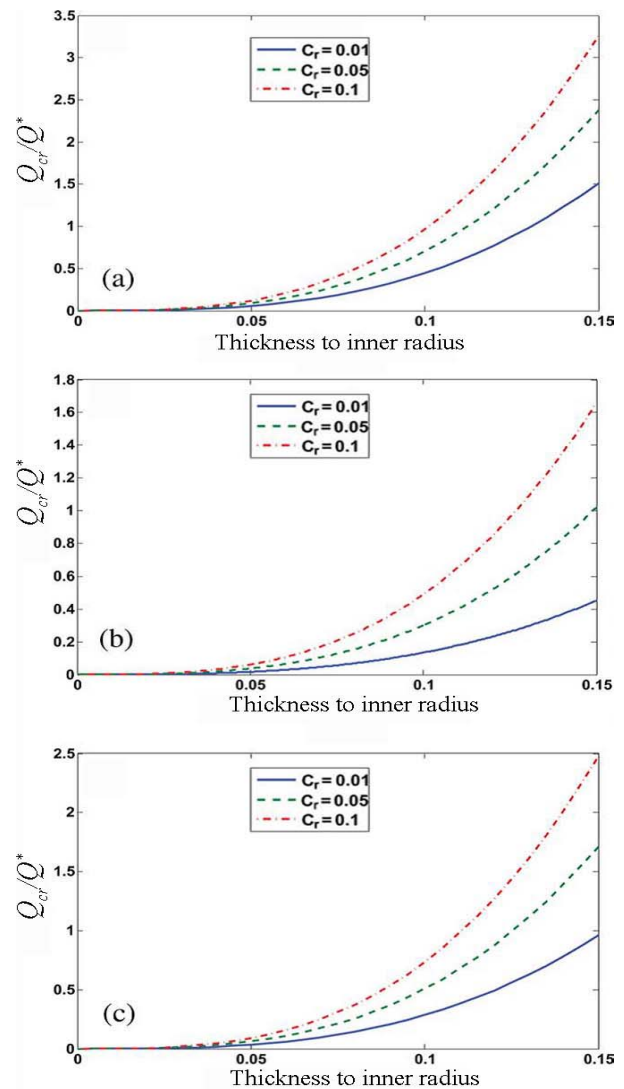


Fig. 3 The effect of thickness to inner radius on the torsional buckling loads of composite circular plate for three CNTs volume fraction and different boundary conditions: a) C-C, b) S-C, c) S-S

The related values of buckling loads shown in Fig. 2 are given in Table 3. As it is observed when the inner to outer radius increases, the plate achieves more stable state. Furthermore, an increase of CNTs volume fraction from 1% to 10% leads to about 56% increase in buckling load for aspect ratio of 0.4. The critical compressive buckling loads obtained with three different methods are shown in Table 4. The results are given for three volume fractions of CNTs. It is clear that the critical compressive buckling load goes up with increasing the CNTs volume fraction. Also the effects of three different kinds of boundary conditions on the buckling loads are perused in Table 4.

Table 2 Comparison between analytical and finite element methods results and the effect of volume fraction and aspect ratio on compressive buckling of plate

Aspect Ratio	CNTs Volume fraction	TSDT P_{cr} (kN)	ANSYS P_{cr} (kN)	CLPT P_{cr} (kN)
a/b=0.1	0.01	635.34	642.24	679.16
	0.05	991.35	980.27	1069.7
	0.1	1402.256	1398.1	1582.9
a/b=0.2	0.01	685.101	671.2	711.5
	0.05	1011.53	980.47	1018.6
	0.1	1312.35	1290.36	1434.48
a/b=0.3	0.01	692.24	680.24	771.83
	0.05	889.74	867.5	1015
	0.1	1310.58	1276.04	1355.9
a/b=0.4	0.01	826.104	801.94	877.23
	0.05	979.36	959.36	1069
	0.1	1260.54	1952.13	1352.4

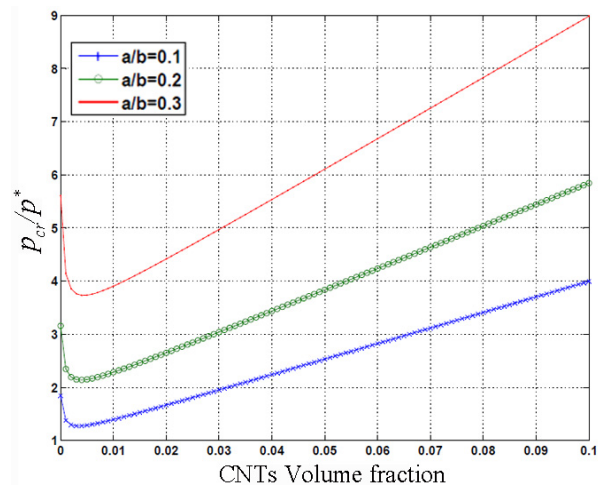


Fig. 4 CNTs volume fraction versus compressive buckling loads for three ratios of inner-to-outer radius

As a result, the highest critical axial buckling load occurs at $C_r=0.1$ for each boundary condition. The results of the analytical method and the two FEMs are quite compatible with each other (Table 2 and Table 4). As seen in the mentioned tables, in most cases the results of TSDT is closer to the analytical solution as compared with the ANSYS results. However, the FEM results show a lower critical buckling load than those calculated by analytical method due to elimination of shear strain in the classical plate theory.

The effect of orientation angle of CNTs on the critical torsional buckling load for three aspect ratios and three boundary conditions is demonstrated in Fig. 6. The plate is in the most stable state as a result of arranging CNTs into circumferential direction.

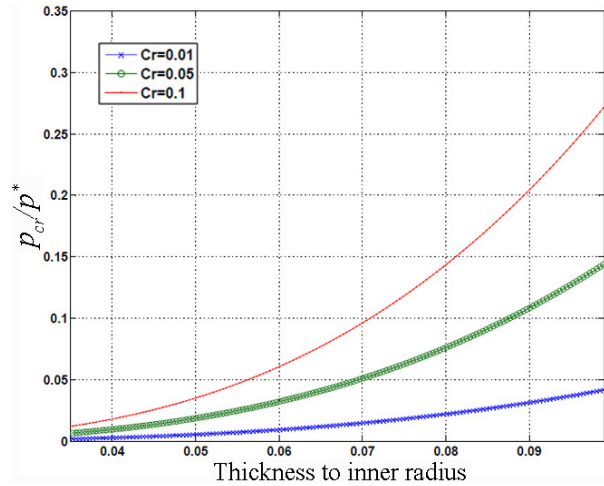


Fig. 5 Thickness-to-inner radius versus the compressive buckling loads for three volume fractions of CNTs

Table 3 The effect of inner to outer radius on the critical torsional buckling loads of annular composite plates, kN/m

Aspect Ratio	$C_r=1\%$	$C_r=5\%$	$C_r=10\%$
a/b=0.1	5.015	7.84	11.961
a/b=0.2	8.23	13.24	18.96
a/b=0.3	17.125	24.067	32.14
a/b=0.4	38.934	46.63	61.003

Table 4 Comparison between analytical and FEM results and the effect of volume fraction and boundary condition on compressive buckling of plate

B.Cs	CNTs Volume fraction	TSDT P_{cr} (kN)	ANSYS P_{cr} (kN)	CLPT P_{cr} (kN)
S - S	0.01	51.241	54.1327	59.546
	0.05	212.84	201.95	218.38
	0.1	401.324	397.268	417
C - S	0.01	110.03	108.957	114.7
	0.05	382.47	379.16	393
	0.1	732.42	727.89	741.03
C - C	0.01	17.304	16.284	19.015
	0.05	63.39	61.14	65.59
	0.1	119.67	118.38	123.83

Since the angle is raised to reach into radial direction, the critical moment falls for all aspect ratios. The higher inner-to-outer ratio leads to a more stable state for each direction of the CNTs. However, the greatest difference between four aspect ratios is acquired when the CNTs are arranged into circumferential direction and it is diminished as the orientation angle rises. Similar to previous figure, critical compressive buckling loads is drawn in Fig. 7 and the effect of nanotubes orientation and different aspect ratios is demonstrated.

The values of torsional buckling loads for angles of 0° , 15° , 30° and 45° and four different aspect ratios are given in Table 5. The most significant difference

between four aspect ratios creates when the CNTs are arranged into circumferential direction and it decrease since the angle is raised to reach into radial direction.

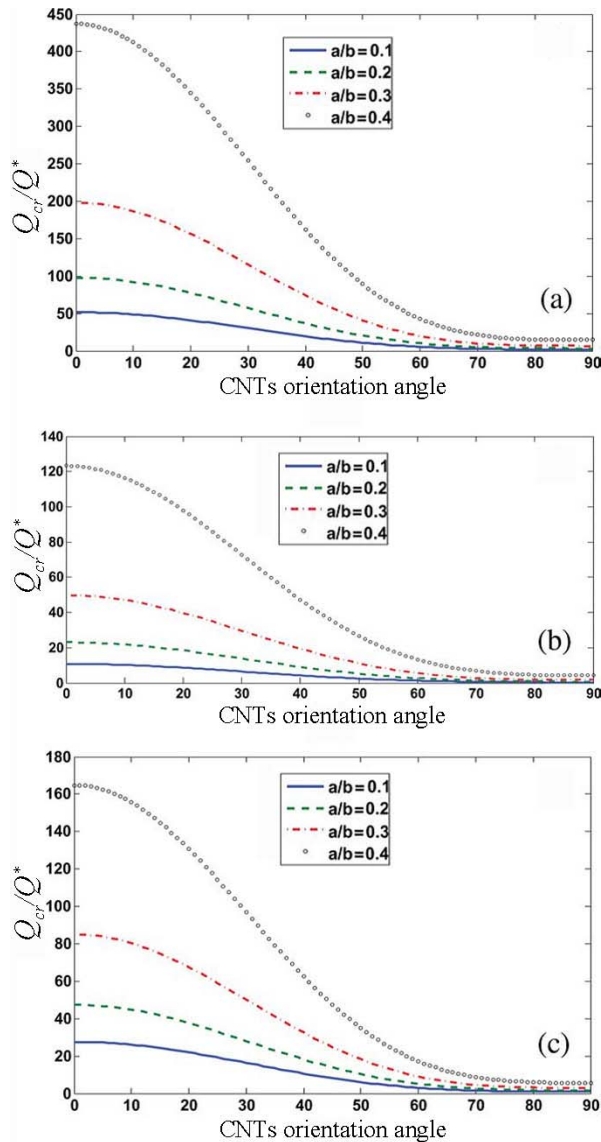


Fig. 6 The effect of nanotubes orientation angle on the torsional buckling load for different aspect ratio and different boundary conditions: a) C-C, b) S-C, c) S-S

Table 5 The effect of CNTs orientation angle and aspect ratio on the torsional buckling loads of annular composite plates, kN/m

Aspect Ratio	$\theta=0^\circ$	$\theta=15^\circ$	$\theta=30^\circ$	$\theta=45^\circ$
$a/b=0.1$	182.38	160.18	107.16	52.72
$a/b=0.2$	346.16	303.8	202.68	99.113
$a/b=0.3$	699.85	613.73	408.33	198.44
$a/b=0.4$	1545	1353.8	898.4	434.06

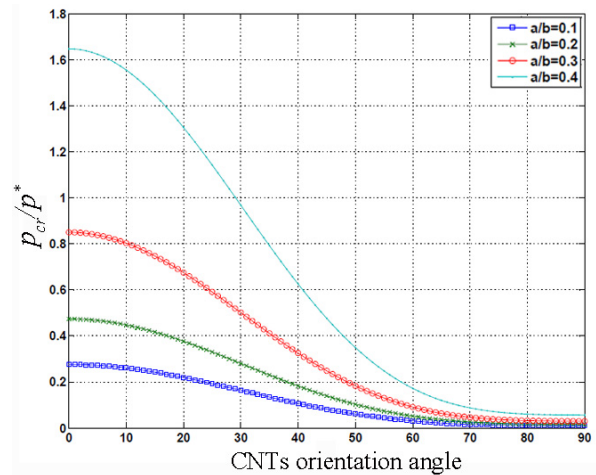


Fig. 7 Orientation angle versus compressive buckling load for different ratios of inner-to-outer radius

6 CONCLUSION

In this article, the buckling analysis of circular/annular composite plates reinforced by CNTs under torsional and compressive loads is presented. Third order shear deformation method accurately predicts the behaviour of CNTs reinforced annular composite plates, whereas the ANSYS and CLPT overestimate buckling loads. It is determined that for all the boundary conditions considered, the inner-to-outer radius ratio of $a/b=0.4$ and the orientation angle of 0° parallel to circumferential direction yield the highest critical buckling load. A circular hole reduces the stability of the plate and the buckling load decreases by increasing the ratio of inner-to-outer radius. The following conclusions may be drawn from the results for both compressive and torsional buckling loads obtained from different solvency methods:

- The critical buckling loads obtained based on the analytical method and the FEMs are quite compatible to each other. In most cases the results of TSDT is closer to the analytical solution as compared with the ANSYS results. The critical buckling loads resulting from analytical method are higher than those for finite element methods because of eliminating shear strain.
- The slope of the buckling load curves increases sharply at high CNTs volume fractions as the thickness of plate rises. Also the plate would be more stable if the ratio of inner-to-outer radius increases.
- For both compressive and torsional loads, it is obvious that the critical buckling load goes up with increasing the CNTs volume fraction. For example, increase of volume fraction from 1% to 10% leads to about 56% increase in buckling load.

- The highest critical buckling load occurs for the case in which both inner and outer edges have clamped support. In addition edges with simply supported conditions on both inner and outer radius cause to lowest critical moment.
- The plate is in the most stable state as a result of arranging CNTs into circumferential direction. However, the greatest difference between different aspect ratios is acquired when the CNTs are arranged into circumferential direction and it is diminished as the orientation angle rises.

REFERENCES

- [1] Popov, V. N., Van Dorena, V. E. and Balkanskib, M., "Elastic properties of crystals of single-walled carbon nanotubes", *Solid State Communications*, Vol. 114, No. 7, 2000, pp. 395-399.
- [2] Jin, Y., Yuan, F.G., "Simulation of elastic properties of single-walled carbon nanotubes", *Compos. Sci. Technol.*, Vol. 63, 2003, pp. 1507-1515.
- [3] Esawi, A. M. K., Farag, M. M., "Carbon nanotube reinforced composites: potential and current challenges", *Materials and design*, Vol. 28, 2007, pp. 2394-2401.
- [4] Liu, Y. J., Chen, X. L., "Evaluations of the effective material properties of carbon nanotube-based composites using a nanoscale representative volume element", *Mechanics of Materials*, Vol. 35, 2003, pp. 69-81.
- [5] Bonnet, P., Sireude, D., Garnier, B. and Chauvet, O., "Thermal properties and percolation in carbon nanotube-polymer composites", *J. Appl. Phys.*, Vol. 91, 2007, pp. 2019-2030.
- [6] Chiu, F. C., Kao, G. F., "Polyamide 46/multi-walled carbon nanotube nanocomposites with enhanced thermal, electrical, and mechanical properties", *Composites: Part A*, Vol. 43, 2012, pp. 208-218.
- [7] Ayatollahi, M. R., Shadlou, S., Shokrieh, M. M. and Chitsazadeh, M., "Effect of multi-walled carbon nanotube aspect ratio on mechanical and electrical properties of epoxy-based nanocomposites", *Polymer Testing*, Vol. 30, 2011, pp. 548-556.
- [8] Birman, V., Bert, C.W., "Buckling of composite plate and shells subject to elevated temperature", *Journal of Applied Mechanics*, Vol. 60, No. 2, 1993, pp. 514-9.
- [9] Najafizadeh, M. M., Eslami, M. R., "Thermoelastic stability of orthotropic circular plates", *Journal of Thermal Stresses*, Vol. 25, No. 10, 2002, pp. 985-1005.
- [10] Najafizadeh, M. M., Hedayati, B., "Refined theory for thermoelastic stability of functionally graded circular plates", *Journal of Thermal Stresses*, Vol. 27, No. 9, 2004, pp. 857-80.
- [11] Krizevsky, G., Stavsky, Y., "Refined theory for vibrations and buckling of laminated isotropic annular plates", *International Journal of Mechanical Sciences*, Vol. 38, No. 5, 1996, pp. 539-55.
- [12] Najafizadeh, M. M., Heydari, H. R., "Thermal buckling of functionally graded circular plates based on higher order shear deformation plate theory," *European Journal of Mechanics A/Solids*, Vol. 23, 2004, pp. 1085-1100.
- [13] Najafizadeh, M. M., Heydari, H. R., "An exact solution for buckling of functionally graded circular plates based on higher order shear deformation plate theory under uniform radial compression," *International Journal of Mechanical Sciences*, Vol. 50, 2008, pp. 603-612.
- [14] Ma, L. S., Wang, T. J., "Relationships between axisymmetric bending and buckling solutions of FGM circular plates based on third-order plate theory and classical plate theory," *International Journal of Solids and Structures*, Vol. 41, No. 1, 2004, pp. 85-101.
- [15] Singhatanadgid, P. Ungbhakorn, V., "Scaling laws for buckling of polar orthotropic annular plates subjected to compressive and torsional loading," *Thin Walled Structures*, Vol. 43, 2005, pp. 1115-1129.
- [16] Saidi, A. R., Rasouli, A. and Sahraee, S., "Axisymmetric bending and buckling analysis of thick functionally graded circular plates using unconstrained third-order shear deformation plate theory," *Composite Structures*, Vol. 89, No. 1, 2009, pp. 110-119.
- [17] Ozakca, M., Taysi, N. and Kolcu, F., "Buckling analysis and shape optimization of elastic variable thickness circular and annular plates- I. Finite element formulation," *Engineering Structures*, Vol. 25, 2003, pp. 181-192.
- [18] Ozakca, M., Taysi, N. and Kolcu, F., "Buckling analysis and shape optimization of elastic variable thickness circular and annular plates- II. Shape optimization," *Engineering Structures*, Vol. 25, 2003, pp. 193-199.
- [19] Shi, D. L., Feng, X. Q., Huang, Y. Y., Hwang, K. C. and Gao, H., "The Effect of Nanotube Waviness and Agglomeration on the Elastic Property of Carbon Nanotube Reinforced Composites," *Journal Engineering Material Technology*, Vol. 126, 2004, pp. 250-257.
- [20] Selmi, A., Friebel, C., Doghri, I. and Hassis, H., "Prediction of the elastic properties of single walled carbon nanotube-reinforced polymers: a comparative study of several micromechanical models," *Compos. Sci. Technol.*, Vol. 67, 2007, pp. 2071-2084.
- [21] Shao, L. H., Luo, R. Y., Bai, S. L. and Wang, J., "Prediction of effective moduli of carbon nanotube-reinforced composites with waviness and debonding," *Compos. Struct.*, Vol. 87, 2009, pp. 274-281.
- [22] Kollar, L. P., Springer, G. S., "Mechanics of Composite Structures", Cambridge University, New York, 2003.
- [23] Vinson, J. R., "The behavior of thin walled structures", beams, plates and shells, Kluwer Academic pub., Netherlands, 1989.
- [24] Reddy, J. N., Khdeir, A. A., "Buckling and vibration of laminated composite plate using various plate theories", *AIAA Journal*, Vol. 27, No. 12, 1989, pp. 1808-17.
- [25] Reddy, J. N., "Theory and Analysis of Elastic Plates", Taylor & Francis, Philadelphia, 1999.
- [26] Reddy, J. N., "An Introduction to the Finite Element Method", McGraw-Hill, New York, 1993.